Pre-Turbulent Regimes in Graphene Flows

M. Mendoza,[1,*] H. J. Herrmann,[1,†] and S. Succi[2,‡]

[1] *ETH Zürich, Computational Physics for Engineering Materials, Institute for Building Materials, Schafmattstrasse 6, HIF, CH-8093 Zürich (Switzerland)*
[2] *Istituto per le Applicazioni del Calcolo C.N.R., Via dei Taurini, 19 00185, Rome (Italy), and Freiburg Institute for Advanced Studies, Albertstrasse, 19, D-79104, Freiburg, Germany*

(Dated: February 6, 2022)

We provide numerical evidence that electronic pre-turbulent phenomena in graphene could be observed, under current experimental conditions, through detectable current fluctuations, echoing the detachment of vortices past localized micron-sized impurities. Vortex generation, due to micron-sized constriction, is also explored with special focus on the effects of relativistic corrections to the normal Navier-Stokes equations. These corrections are found to cause a delay in the stability breakout of the fluid as well as a small shift in the vortex shedding frequency. Finally, a relation between the Strouhal number, a dimensionless measure of the vortex shedding frequency, and the Reynolds number is provided under conditions of interest for future experiments.

PACS numbers: 72.80.Vp, 47.75.+f, 47.11.-j
Keywords: Graphene, relativistic fluid dynamics, Dirac particles, lattice Boltzmann

Since its recent discovery [1, 2], graphene has continued to surprise scientists with an amazing series of spectacular properties, such as ultra-high electrical conductivity, ultra-low viscosity to entropy ratio, combination of exceptional structural strength and mechanical flexibility, and optical transparency. Many of these fascinating effects are due to the fact that, consisting of literally a single carbon monolayer, graphene represents the first instance of a truly two-dimensional material (the "ultimate flatland" [3]). Moreover, due to the special symmetries of the honeycomb lattice, electrons in graphene are shown to behave like an effective Dirac fluid of *massless* chiral quasi-particles propagating at a Fermi speed of about $v_F \sim c/300 \sim 10^6$ m/s. This configures graphene as a very special, slow-relativistic electronic fluid, where many unexpected quantum-electrodynamic phenomena can take place, [4–6]. In particular, the capability of reaching down viscosity to entropy ratios smaller than that of superfluid Helium at the lambda-point, has recently spawned the suggestion that electronic transport in graphene may support pre-turbulent phenomena, Ref. [7].

In this Letter, we pursue this suggestion in quantitative terms. More precisely, we simulate the relativistic graphene-fluid equations, proposed in Ref. [7], under conditions of present and prospective experimental realizability. Our main result is that micro-scale impurities, as small as a few microns, are capable of triggering coherent patterns of vorticity in close qualitative and quantitative resemblance with classical two-dimensional turbulence (see e.g. Fig. 1). It is also shown that such vorticity patterns give rise to detectable current fluctuations across the sample, well in excess of flickering noise. As a result, based on our simulations, we conclude that the hydrodynamic picture of graphene as a near-perfect, slow-relativistic fluid, as developed in Ref. [7], should be liable to experimental verification. The equations for the Dirac electron fluid in graphene read as follows [7]: $\partial\rho_c/\partial t + \nabla\cdot(\rho_c\vec{u}) = 0$, for charge conservation; $\partial\epsilon/\partial t + \nabla\cdot[(\epsilon+p)\vec{u}] = 0$, for energy density conservation and

$$\frac{\epsilon+p}{c^2}\left[\frac{\partial\vec{u}}{\partial t} + (\vec{u}\cdot\nabla)\,\vec{u}\right] + \nabla p + \frac{\vec{u}}{c^2}\frac{\partial p}{\partial t} - \eta\nabla^2\vec{u} = 0 \quad , \quad (1)$$

for momentum conservation. Here, c is the Fermi speed ($\sim 10^6$m/s), ϵ the energy density, p the pressure, ρ_c the charge density, and $\vec{u}$ the velocity. The shear viscosity

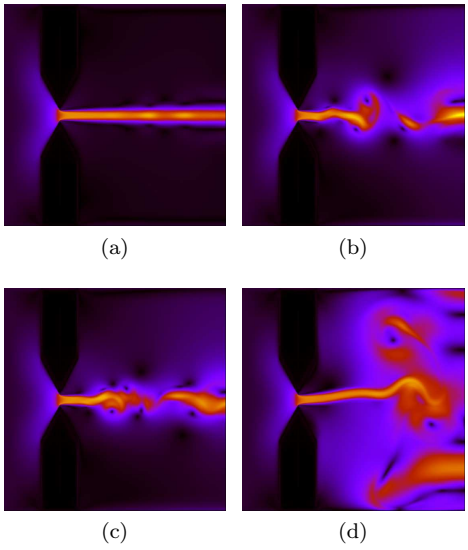

FIG. 1: Pre-turbulence at Reynolds number $Re = 25$ in graphene is shown: at 379400 time steps, (a) and (b); and at 603400 time steps, (c) and (d). For (b) and (d) the term $\partial p/\partial t$ was removed. The color represents the magnitude of the velocity.

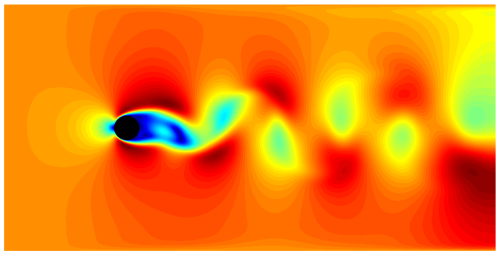

FIG. 2: Vortex shedding in graphene at Reynolds number $Re = 100$, using a grid of 1024×512 cells. The color scale represents the absolute velocity of the fluid. The picture was taken at 4×10^6 time steps.

can be calculated by using [7]

$$\eta = C_\eta \frac{N(k_B T)^2}{4\hbar c^2 \alpha^2} \quad , \tag{2}$$

where $C_\eta \sim O(1)$ is a numerical coefficient, T is the temperature, $\alpha = e^2/\varepsilon\hbar c$ is the effective fine structure constant, e being the electric charge of the electron, ε the relative dielectric constant, and N the number of species of free massless Dirac particles. Additionally, the entropy density can be calculated according to the Gibbs-Duhem relation $\epsilon + p = Ts$. These equations have been derived under the assumption $|\vec{u}| \ll c$.

The relativistic lattice Boltzmann (RLB), proposed by Mendoza et. al. [8, 9], is hereby adapted to reproduce, in the continuum limit, the equations for the Dirac electron fluid described above. The RLB model [8] was defined on a three-dimensional lattice with nineteen discrete velocities. Since graphene is $2D$, we have adapted the model to a two-dimensional cell with nine discrete velocities, linking each site to its four nearest-neighbors, four next-to-nearest neighbors (diagonal), plus a rest particle. Two distribution functions, f_i and g_i, are used for the particle number and momentum-energy, respectively. These distribution functions evolve according to the typical Boltzmann equation in single-time relaxation approximation [8, 10], $f_i(x + \delta x, t + \delta t) - f_i(x, t) = -(f_i - f_i^{\rm eq})/\tau$ and $g_i(x + \delta x, t + \delta t) - g_i(x, t) = -(g_i - g_i^{\rm eq})/\tau$, where τ is the single relaxation time, and the equilibrium functions $f_i^{\rm eq}$ and $g_i^{\rm eq}$ are defined in Ref. [8, 9]. The shear viscosity, according to this model is $\eta = (\epsilon + p)\left(\tau - \frac{1}{2}\right) c_l^2 \delta t/3c^2$, where $c_l = \delta x/\delta t$ is the ratio of the lattice spacing to time-step size.

We choose the equation of state $\epsilon = 3p$, which depends on temperature in the relativistic regime, as $\epsilon \sim (k_B T)^3/(c\hbar)^2 = T^3$ (in normalized units $c = \hbar = k_B = e = 1$) [11]. Thus, the shear viscosity η would depend on the third power of the temperature, leading to a different relation than Eq. (2). However, in the Dirac fluid, the relaxation time for the electrons depends on the inverse of the temperature, $\tau_{rel} = (\hbar\alpha)^2/k_B T$ [12], and, therefore, introducing this dependence into the relaxation time τ of the numerical model, we obtain the correct function for the viscosity. In numerical units ($\delta x = \delta t = c = 1$), we set the relaxation time to $\tau = \tau_0 T_0/T + 1/2$, where T_0 is the initial temperature and τ_0 the initial relaxation time.

The hydrodynamics equations are similar to the non-relativistic Navier-Stokes equations with the exception of the compressibility term $\sim \partial p/\partial t$. This term is most likely negligible at low frequencies, but it may become relevant at higher ones. The Reynolds number Re, measuring the strength of inertial versus dissipative terms [7], is given by $Re = (sT/c^2)(LU_{typ}/\eta)$, where L and U_{typ} are the characteristic length and flow velocity of the system, respectively. In lattice units, it reads as

$$Re = \frac{3LU_{typ}}{c^2 \delta t \left(\tau - \frac{1}{2}\right)} \quad . \tag{3}$$

According to classical turbulence theory, vortex shedding in graphene is expected for Reynolds numbers well above one, typically $Re \sim 10 \div 100$. To detect signatures of pre-turbulent behavior in graphene experiments, one can measure the fluctuations of the electric current through the graphene sample. The current density is defined by $\vec{j} = \rho_c \vec{u}$, and the total electric current is calculated integrating the current density along the transverse (y) coordinate. The characteristic fluctuation frequency can then be related to the vortex shedding frequency. Macroscopic speeds $u \sim 10^5$ m/s could be achieved by the electrons in graphene[13]. The Reynolds number rewrites as: $Re = U_{typ} LT/c^2(\eta/s)$. According to Ref. [7], η/s takes values around $0.2\hbar/k_B$, at temperature of 300K, so that we can write $Re = U_{typ} L/\nu_{eff}$, $\nu_{eff} = c^2\eta/Ts \sim 0.005$ m^2/s being the effective kinematic viscosity. Therefore, a sample of size $L = 5\mu$m, within reach of current technology, would yield $Re \sim 100$, sufficiently high to trigger pre-turbulent phenomena, such as vortex shedding. To test the idea on quantitative grounds, we implement a simulation on a grid with 1024×512 cells. The following initial values (numerical units) were used: $\epsilon = 0.75$, $\rho_c = 1.0$, $\vec{u} = (u_x, 0) = (0.002, 0)$, and the Fermi speed $c = c_l = 1.0$. The initial value of the relaxation time was chosen $\tau_0 = 0.003$ such that the initial shear viscosity $\eta = \frac{1}{3}\left(\tau - \frac{1}{2}\right) = 10^{-3}$.

A circular obstacle, with diameter $D = 50$, is introduced at $(256, 256)$, modeling a 5 micron diameter impurity in the graphene sample (Fig. 2). With this configuration, and setting $L = D$ in Eq. 3, the Reynolds number for this system is $Re \sim 100$. We choose periodic boundary conditions at top and bottom, and demand that the distribution functions of the boundary cells are always equal to the equilibrium distribution functions evaluated with the initial conditions. Free boundary conditions are imposed at the outlet. At the left border, we set inlet conditions, where the missing information of the distribution functions is filled by the equilibrium distribution function corresponding to the initial conditions [14]. We define $\delta t = 0.05$ps.

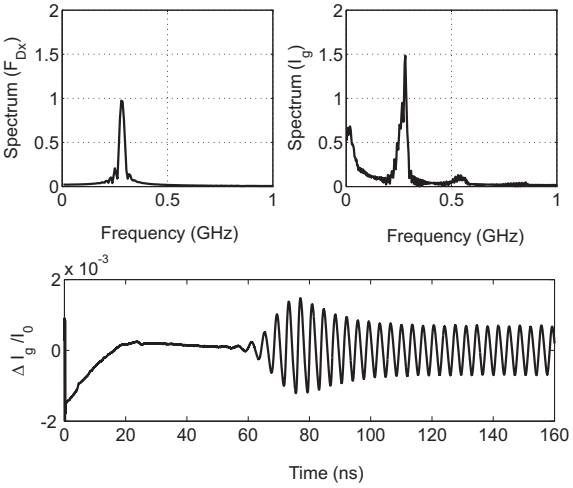

FIG. 3: FFT of the electric current fluctuations ΔI_g, in the graphene sample (top right), due to the vortex shedding as a function of time. Also, it is shown the FFT of the drag force acting on the obstacle (top left). This result refers to $Re = 100$. At the bottom, the fluctuations in the electric current I_g are shown as a function of time.

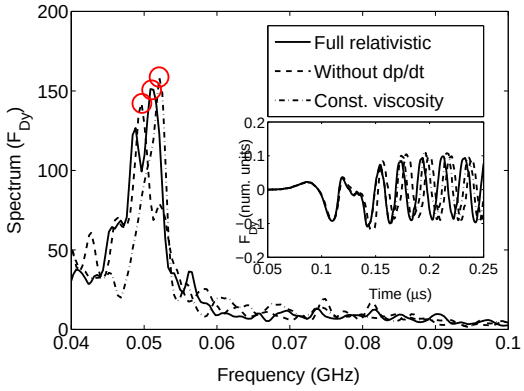

FIG. 4: Frequencies of the vortex shedding at Reynolds number $Re = 3000$, using a grid of 2048×1024 cells, are shown. These are calculated for three different cases: the full relativistic, relativistic without the term $\partial p/\partial t$, and relativistic with constant viscosity.

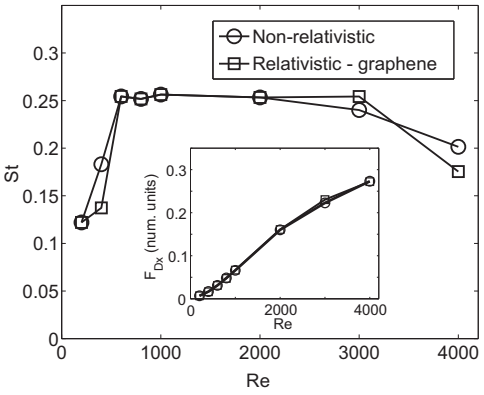

FIG. 5: Strouhal number St as a function of the Reynolds number Re for both non-relativistic and relativistic fluids. In the inset, the mean value of the x-component of the drag force as a function of the Reynolds number is shown. The error bar is of the size of the symbol.

The drag F_{Dx} and lift F_{Dy} forces acting on the obstacle are measured, the vortex shedding frequency being computed in terms of fluctuations of the lift forces. We compare the frequency of the electric current fluctuations with the frequency of the drag force, which, in general, is twice the vortex shedding frequency (see Fig. 3). To relate these to the vortex shedding, we use a fast-Fourier transform (FFT). As is well visible from Fig. 3, the current fluctuations contribute about one part per thousand of the base signal, and, consequently, they should be liable to experimental detection. In future applications, involving larger graphene samples, higher Reynolds numbers will be attained. Consequently, it becomes of interest to assess the role of the relativistic corrections to the classical Navier-Stokes equations.

Comparing the dynamics of the relativistic and non-relativistic fluids, two basic differences emerge: the relativistic correction term $\sim \partial p/\partial t$; and the viscosity dependence with the temperature, Eq. (2). In order to assess whether these terms play an important role, we implement three simulations on a grid of size 2048×1024 cells. In the first simulation, we model the full relativistic equations; in the second one, the relativistic effect $\sim \partial p/\partial t$ is removed; and in the third one, the viscosity is forced to be a constant. The same initial configuration, as before, is used with the exception of: $\vec{u} = (u_x, 0) = (0.03, 0)$ and $D = 100$ (in this case, modeling an impurity of diameter 150μm). The impurity is now centered at $(512, 512)$. With this configuration, Eq. 3 gives $Re \sim 3000$. The simulations run up to 10^6 time steps (with $\delta t = 1.5$ps).

From Fig. 4, we find that, in the case of constant viscosity, the frequency is a bit higher than the one corresponding to the full relativistic case. On other hand, if the term $\sim \partial p/\partial t$ is removed from the equations, the frequency decreases. We conclude that, in order to compare to high precision measurements of the vortex shedding frequencies, these terms cannot be ignored. To study the frequency of the vortex shedding, we vary the initial velocity in order to obtain different Reynolds numbers. The Strouhal number St is defined as the dimensionless frequency of the vortex shedding and can be calculated as $St = f_s L/U_{typ}$, where f_s is the frequency of the vortex shedding. Fig. 5 shows that the relation between St and Re is very similar for the relativistic and non-relativistic fluids, with a fast growth of St in the range $200 < Re < 1000$, followed by a flat-top at $St \sim 0.25$ [15–17] for $Re > 1000$. From the Strouhal number, we can obtain the frequencies of the vortex shedding, as $f_s = 0.2U_{typ}/L$. The frequency of the drag force is twice that of vortex shedding, namely $f_{Ds} = 0.4U_{typ}/L$. As

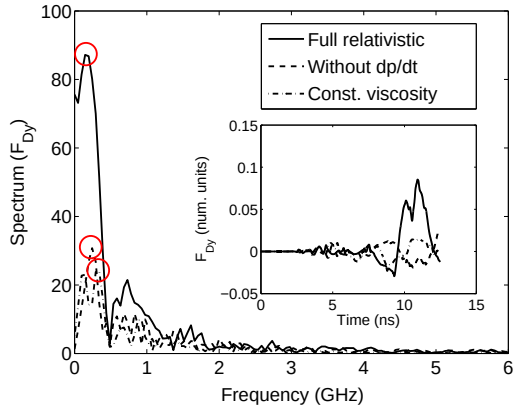

FIG. 6: The same case of Fig. 4, but in the case of the constriction at Reynolds number $Re = 25$, using a grid with 1024×1024 cells.

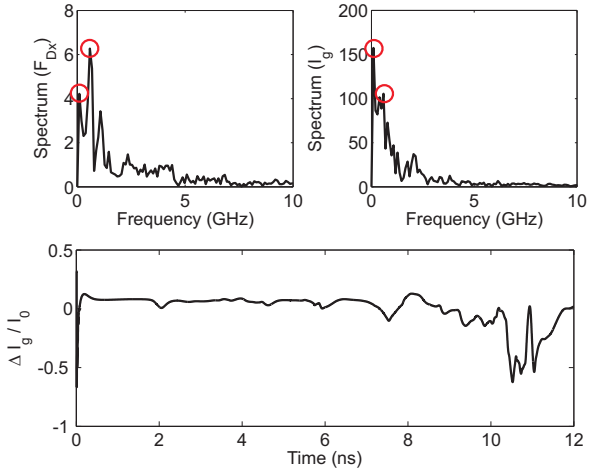

FIG. 7: The same case as Fig. 3 for the constricted flow at $Re = 25$.

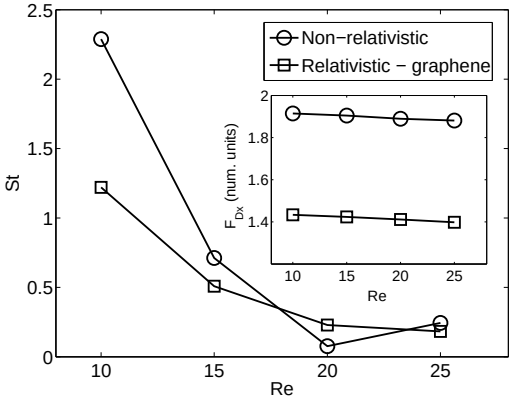

FIG. 8: The same as Fig. 5 for the case of the constriction.

a result, once the Reynolds number is known, one can compute the frequency of the drag force, the Strouhal number, and then compare with the FFT of the electric current measurement in the sample. The mean value of the drag force $\overline{F}_{Dx}$, reported in the inset of Fig. 5 as a function of the Reynolds number, shows a monotonic dependence in the range of Re explored here.

Another kind of set-up to detect pre-turbulence in graphene experiments, with the possibility of being implemented nowadays, consists of building a constriction, where the Dirac fluid can develop vorticity patterns as it crosses through. Fig. 1 shows the vorticity at $Re = 25$, where the characteristic length $L = 50$ cells has been chosen as the distance between the tips. In this case, the initial velocity is taken $\vec{u} = (u_x, 0) = (0.0005, 0)$, in lattice units, and the simulation is performed using a grid of 1024×1024 cells. We simulate two systems, one with the full relativistic equations and the other one by just removing the relativistic term $\partial p/\partial t$. From the simulations (see Fig. 1), we conclude that the relativistic contribution affects the time to the onset of instability, and, from Fig. 6, we can appreciate that, as for the circular impurity, the frequency of the vortices presents a shift due to the relativistic corrections. However, both constant viscosity and removal of the relativistic correction, contribute to an increase of the frequency of the fluctuations. Fig. 7 shows how such fluctuations can be measured, and the characteristic frequencies (see red circles in Fig. 7) related with the drag force acting on the constriction. Note that, in order to achieve $Re = 25$, at a speed of $0.1c$, the distance between tips is about 1.25μm.

As for the case of the circular impurity, we can find the characteristic relation between the Strouhal number and the Reynolds number for this geometrical set-up (see Fig. 8). From the inset of Fig. 8, we observe that the drag force decreases slightly, as the Reynolds number is increased, and exhibits a noticeable difference between the non-relativistic and relativistic cases.

Summarizing, we have shown that, in the range of $Re \sim 10^2$, vorticity patterns can be indirectly observed by measuring the electric current fluctuations in the graphene sample. However, using a different geometry, like a constriction, signatures of pre-turbulence can be detected already at Reynolds numbers as small as $Re \sim 25$. We have also compared the effects of relativistic corrections, such as dynamic compressibility and the dependency of the viscosity on the temperature, on the dynamics of the system. In these cases, the temperature dependency of the viscosity and the term $\partial p/\partial t$ produce a shift in the frequencies of the vortex shedding and, therefore, in the electric current fluctuations. Additionally, the relativistic correction term, $\sim \partial p/\partial t$, is found to delay the instability process in the case of the constricted flow. For future applications, most likely accessing higher Reynolds numbers, the frequency of the vortex shedding can be calculated using the Strouhal number,

thereby permitting to distinguish current fluctuations induced by pre-turbulent phenomena from those resulting from other physical effects.

We thank K. Ensslin for enlightening discussions.

* Electronic address: mmendoza@ethz.ch
† Electronic address: hjherrmann@ethz.ch
‡ Electronic address: succi@iac.cnr.it

[1] K. Novoselov, A. Geim, S. Morozov, D. Jiang, M. Katsnelson, I. Grigorieva, and S. Dubonos, Nature Letters **438**, 197 (2005).
[2] K. S. Novoselov, A. K. Geim, S. V. Morozov, D. Jiang, Y. Zhang, S. V. Dubonos, I. V. Grigorieva, and A. A. Firsov, Science **306**, 666 (2004).
[3] A. K. Geim and A. H. MacDonald, Phys. Today p. 35 (2007).
[4] E. Shuryak, Progress in Particle and Nuclear Physics **53**, 273 (2004), ISSN 0146-6410, heavy Ion Reaction from Nuclear to Quark Matter.
[5] P. K. Kovtun, D. T. Son, and A. O. Starinets, Phys. Rev. Lett. **94**, 111601 (2005).
[6] G. Policastro, D. T. Son, and A. O. Starinets, Phys. Rev. Lett. **87**, 081601 (2001).
[7] M. Müller, J. Schmalian, and L. Fritz, Phys. Rev. Lett. **103**, 025301 (2009).
[8] M. Mendoza, B. M. Boghosian, H. J. Herrmann, and S. Succi, Phys. Rev. Lett. **105**, 014502 (2010).
[9] M. Mendoza, B. M. Boghosian, H. J. Herrmann, and S. Succi, Phys. Rev. D **82**, 105008 (2010).
[10] P. Bhatnagar, E. P. Gross, , and M. Krook, Phys. Rev. **94**, 511 (1954).
[11] S. A. Hartnoll, P. K. Kovtun, M. Müller, and S. Sachdev, Phys. Rev. B **76**, 144502 (2007).
[12] L. Fritz, J. Schmalian, M. Müller, and S. Sachdev, Phys. Rev. B **78**, 085416 (2008).
[13] I. Meric, M. Y. Han, A. F. Young, B. Ozyilmaz, P. Kim, and K. L. Shepard, Nature Nanotech. **3**, 654 (2008).
[14] S. Succi, *The Lattice Boltzmann Equation for Fluid Dynamics and Beyond* (Oxford University Press, USA, 2001), ISBN 0198503989.
[15] C. H. K. Williamson, Journal of Fluid Mechanics **206**, 579 (1989).
[16] C. H. K. Williamson, Physics of Fluids **31**, 3165 (1988).
[17] F. L. Ponta and H. Aref, Phys. Rev. Lett. **93**, 084501 (2004).